Journal of Hydrology 526 (2015) 89–100

Contents lists available at ScienceDirect

Journal of Hydrology

journal homepage: www.elsevier.com/locate/jhydrol

Analyzing the sensitivity of drought recovery forecasts to land surface initial conditions

Caleb M. DeChant, Hamid Moradkhani *

Department of Civil and Environmental Engineering, Portland State University, United States

ARTICLE INFO

Article history:
Available online 23 October 2014

Keywords:
Drought recovery
Ensemble forecasting
Data assimilation

SUMMARY

Droughts are complex hydro-meteorological phenomena, which are challenging to both quantify and predict. From the perspective of drought quantification, knowledge of the land surface conditions is vital for determining the impacts a drought event is having on both the environment and society. Although such land surface information is essential for quantifying drought in real-time, the precise effect of land surface moisture deficits on future drought conditions is unknown. Forecasting of recovery from drought events is undoubtedly reliant on its intensity, yet the lead time at which a drought can be expected to recover is poorly understood. Due to this gap in knowledge, this study attempts to quantify the expected lead time for drought recovery, and the rate of drought recovery, by examining the loss of sensitivity to initial conditions within a climatological forecast. From this perspective, the expected recovery time from a specific drought event is quantified, based on a case study in the Upper Colorado River Basin in Southwestern USA for two initialization dates in years 2003 through 2008. This study has ramifications for understanding the time of drought recovery, and highlights the importance of accurate land surface state estimation. With respect to recent studies, the experiments presented here suggest that forecasts can be sensitive to initial conditions at greater lead-times, and therefore drought conditions are potentially more persistent than previously thought.

1. Introduction

Forecasting of land surface states at seasonal to annual lead times is essential for drought management, providing a basis for applying mitigation measures (Pozzi et al., 2013). Through effective application of such mitigation measures, the impacts of drought may be reduced, making drought forecasts critical for reducing economic losses (Huang and Chou, 2008; Maity et al., 2013). Although these forecasts are vital to minimizing the cost of drought events, forecasts at seasonal to annual lead times are plagued with low accuracy. As a result of the spatiotemporal complexities of hydro-meteorological states, both observation and simulation of drought relevant variables are challenging (Andreadis and Lettenmaier, 2006a; Hao and AghaKouchak, 2013; Mo et al., 2012). Such a challenge has left scientist with an incomplete understanding of land-atmospheric processes, leading to persistent uncertainties. Due to the perpetuity of uncertainties, it has become widely accepted that forecasts must be framed from a probabilistic perspective (Brown et al., 2010; DeChant and Moradkhani, 2014; Demargne et al., 2013; Madadgar and Moradkhani, 2013b; Yuan et al., 2013), thus relying on statistical principles to convey the level of certainty which one can place on a forecast. From the probabilistic perspective, a forecast user may leverage a given forecast of risk to minimize potential cost of a drought event. In order to perform such risk management, reliable estimates of forecast uncertainty are essential, with increasing effectiveness as the variance of the probabilistic forecast is decreased.

Three primary sources of uncertainty are present in a drought forecasting framework: initial condition, meteorological forcing and model uncertainties. Initial condition uncertainty arises due to the difficulty of estimating land surface water storages at the initial forecast date, meteorological forcing is uncertain due to the imperfect knowledge of climatic conditions over the forecast period, and model uncertainty results from the imperfect nature of land surface models and insufficient information to precisely estimate parameters. Of these three sources of uncertainty, meteorological forcing and model uncertainties are significant at all potential lead times. Alternatively, the initial condition will only be significant up to a certain forecast lead time, with the sensitivity of the forecast to the initial condition reducing as lead time increases (Wood and Lettenmaier, 2008). This scenario makes quantifying the sensitivity of future land surface states to initial

* Corresponding author.
E-mail addresses: cdechant@pdx.edu (C.M. DeChant), hamidm@pdx.edu (H. Moradkhani).

http://dx.doi.org/10.1016/j.jhydrol.2014.10.021
0022-1694/

conditions highly valuable for forecasters and hydro-meteorologists. Two specific examples of this are highlighted in this study: (1) examining the recovery time from a drought scenario and (2) understanding the extent to which improved initial conditions will help a given forecast system.

Understanding the relationship between the intensity of drought conditions and the time to recovery is of great importance (Mishra and Singh, 2010; Pan et al., 2013; Madadgar and Moradkhani, 2013a, 2014). Since a drought is determined by some deficiency in water, that deficiency will take some amount of time to be alleviated. If the magnitude of that deficiency can be related to the expected recovery time, then mitigation measures may be focused during that expected drought recovery period. Without information about future climate, which is commonly assumed in hydrologic forecasting, it is beneficial at the basic level to quantify the recovery time under normal conditions. This provides another view to drought intensity, beyond simply explaining the magnitude of the deficiency. Such information about the typical recovery time may be more functional to the general public and water resources managers alike, and therefore is of interest to society in general. Further, information about sensitivity to initial conditions is useful in considering potential methods to improve a given forecast system as well.

Improving a forecast system involves reducing the uncertainty in initial condition, meteorological forcing, or the model itself. Among these forecast components, uncertainty related to initial condition has great potential to be reduced through recently developed data assimilation techniques. Due to a range of studies in improving estimates of land surface states through data assimilation (Clark et al., 2008; DeChant and Moradkhani, 2011b; Leisenring and Moradkhani, 2011; Margulis et al., 2002; Reichle et al., 2002), particularly with remote sensing data (Andreadis and Lettenmaier, 2006b; DeChant and Moradkhani, 2011a; De Lannoy et al., 2012; Durand et al., 2008), nearly all regions of the planet have the potential for improved land surface state characterization. Although implementation of a data assimilation system has been proven to reduce uncertainty in land surface state, and therefore initial condition, it does require significant resources to develop and maintain. Given this scenario, information about the sensitivity of forecasts in a given basin to initial conditions, at various lead times, would be highly beneficial in the development of forecast systems. If the forecast at the desired lead time is insensitive to the initial conditions, implementation of a data assimilation system may not be warranted. Alternatively, persistent influence of initial condition over the forecast at long lead times would indicate that a data assimilation system is highly beneficial.

A primary objective in this study is determining the sensitivity of drought forecasts to initial conditions, particularly the lead time at which a forecast becomes insensitive to initial conditions. Recently, several studies have analyzed the sensitivity of extended forecasts to initial condition, but have focused on the relative uncertainties in initial condition and meteorological forcing (Li et al., 2009; Mahanama et al., 2011; Paiva et al., 2012; Shukla and Lettenmaier, 2011; Shukla et al., 2013; Yossef et al., 2013). These studies either compared the Ensemble Streamflow Prediction (ESP) methodology (Franz et al., 2008) (deterministic initial conditions with climatological forcing) with Reverse Ensemble Streamflow Prediction (RESP) (stochastic initial conditions with deterministic forcing) (Wood and Lettenmaier, 2008), or examined of the ratio of the variability of initial condition and precipitation during the forecast period. Through these methodologies, it was generally shown that forecasts in snow dominated basins were controlled by initial conditions between three and six month lead times, when the initial forecast date occurred during the accumulation or ablation season, yet only forecasts for very large non-snow dominated basins were controlled by initial conditions beyond a single month. While this analysis provides a compelling argument for the use of data assimilation in short-term forecasts for all basins, and seasonal forecasts during spring and summer for snow dominated basins, such analysis falls short of determining the lead time at which initial condition provide significant information. For example, forcing may be the dominant source of forecast skill beyond the seasonal time-scale for nearly all basins, but initial conditions may still have a significant impact on forecast uncertainty at longer lead times. Due to this shortcoming, this study attempts to quantify the time at which a forecast becomes entirely insensitive to initial condition, and examines the rate at which the information from the initial condition is lost over time. By quantifying the specific lead time at which a forecast is no longer sensitive to initial condition, a forecaster can provide clear evidence of the point at which data assimilation will be of no benefit, and provide insight into the recovery time expected from certain drought events. For the remainder of this study, the term "drought recovery" will be used to describe the loss of sensitivity to initial conditions, and to specify that this study focuses entirely on the effects of land surface moisture deficits on seasonal to annual forecasting, as opposed to moisture surpluses.

2. Methods

2.1. Study area

This study is performed over the entire upper Colorado River basin (UCRB), defined as the entire basin upstream of Lee's Ferry, Arizona (Fig. 1). This basin is semi-arid, with the majority of precipitation falling in the higher elevations as snow, and interior lowlands receiving very little precipitation annually. Although this basin is semi-arid, a large population relies on its runoff. With mean yearly natural flow of 18 billion cubic meters, it supplies water for nearly 26 million people, making the resource extremely strained. In addition to water within the UCRB being a taxed resource, the basin has been prone to drought in recent years, experiencing drought through much of the 21st century. Due to the combination of water supply stress and frequent drought conditions, the UCRB is ripe for study of drought processes.

2.2. Model and data

Experiments performed in this study used the Variable Infiltration Capacity (VIC) model (Gao et al., 2010; Liang et al., 1994). The VIC model is a physically-based, distributed model that solves the energy and water balance at the land surface, which is run at spatially discretized units on a regular grid. A primary feature of VIC is the ability to model sub-grid variability in vegetation and elevation by partitioning the model discretized units into different vegetation types and elevation bands. By accounting for sub-grid variability, the VIC model is well suited for large scale applications. VIC simulations in this study were performed at a spatial resolution of 0.25°. Soil information for VIC simulations were gathered from the Natural Resources Conservation Services STATSGO dataset and vegetation data was gathered from the University of Maryland land cover dataset, derived from observations made by the Advanced Very High Resolution Radiometer (AVHRR).

The VIC model requires precipitation, maximum and minimum temperature, potential evapotranspiration, wind speed, humidity, and incoming shortwave and longwave radiation to perform land surface simulations. Observed precipitation and temperature data was gathered from the NWS Cooperative Observer Program (COOP) and NRCS SNOTEL sites, and then spatially distributed over the UCRB with the aid of Parameter-elevation Regressions on Independent Slopes Model (PRISM) monthly data (Daly et al., 1994). NCEP/

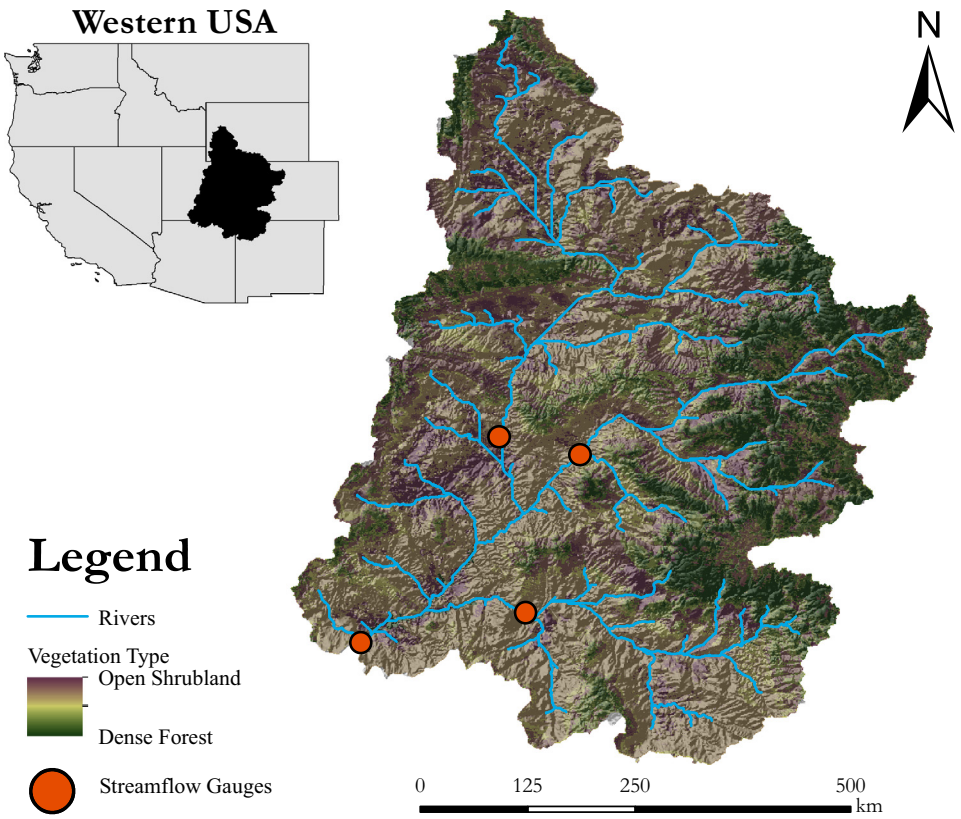

Fig. 1. Map of the upper Colorado River Basin, with shaded elevation relief and vegetation distribution. Major rivers are displayed with the blue lines and the four gauges used for calibration are shown. (For interpretation of the references to colour in this figure legend, the reader is referred to the web version of this article.)

NCAR reanalysis wind data (Kalnay et al., 1996) was gathered and scaled similar following the methods in Maurer et al. (2002). Humidity is estimated according to Kimball et al. (1997), shortwave radiation is estimated according to Thornton and Running (1999), and longwave radiation is estimated according to Bras (1990), which are performed internally in the VIC model.

2.3. Data assimilation

Accurate forecasting of drought recovery requires reliable estimates of the initial drought conditions. Due to the inherent uncertainty in land surface hydrologic states, it becomes necessary to quantify that uncertainty. By quantifying the uncertainty with respect to the land surface states, the forecast becomes more reliable (DeChant and Moradkhani, 2011b). This study relies on estimates of land surface states from the Particle Filter, using sequential importance resampling, for assimilating remotely sensed passive microwave brightness temperature, gathered from the Advanced Microwave Scanning Radiometer (AMSR-E), and land surface temperature from the Moderate Resolution Imaging Spectroradiometer (MODIS). Passive microwave brightness temperature was assimilated at the 6.9, 18.7 and 36.5 GHz channels, as these frequencies exhibit sensitivities to soil moisture and snow water equivalent. Microwave emission modeling was performed with a combination of the Microwave Emission Model for Layered Snowpack (Wiesmann and Mätzler, 1999), the vegetation model from Pulliainen et al. (1998), and the soil component of the L-band Microwave Emission Model (Wigneron et al., 2007). In conjunction with passive microwave brightness temperature, land surface temperature was assimilated to ensure accurate energy state estimates, and improved radiative transfer calculations. The assimilation experiment was performed with 100 ensemble members from October 1st, 2002 through July 1st 2008, providing an ensemble of initial conditions at each forecast starting date of this study.

Ensemble data assimilation requires viewing the model through the state-space framework, described in Eqs. (1) and (2).

$$x_{i,t}^{-} = f(x_{i,t-1}^{+}, u_{i,t}, \theta) \tag{1}$$

$$y_{i,t} = h(x_{i,t}^{-}, \alpha) + v_{i,t} \tag{2}$$

In the above equations, prior model states ($x_{i,t}^{-}$), for ensemble member i at time t, are estimated by integrating the model forward in time, over the posterior states at the previous time step ($x_{i,t-1}^{+}$), the perturbed forcing data ($u_{i,t}$) and the land surface hydrologic parameters (θ). These prior states become the forecast initial conditions when t is the forecast start date (DeChant and Moradkhani, 2011b). If t is during the spin-up period, the radiative transfer model ($h(\cdot)$) must be integrated over the prior states and the land surface radiative parameters (α) to simulate the satellite observations. From this radiative transfer model, the satellite observations ($y_{i,t}$) are simulated, with some predictive error ($v_{i,t}$), allowing for assimilation of those observations. The PF is applied with sequential Bayes Law (Eq. (3)) to estimate the posterior state distribution.

$$p(x_t|y_{1:t}) = \frac{p(y_t|x_t)p(x_t|y_{1:t-1})}{\int p(y_t|x_t)p(x_t|y_{1:t-1})dx} \tag{3}$$

Eq. (3) shows the development of a posterior distribution of model states, given all past remotely sensed observations ($y_{1:t-1}$). Sequential Bayes Law states that the posterior is estimated by the normalized product of the prior distribution ($p(x_t|y_{1:t-1})$) and the likelihood ($p(y_t|x_t)$). Note that $p(x_t|y_{1:t-1})$ is equivalent to $x_{i,t}^{-}$ based on the

importance density chosen here, and the likelihood is Gaussian, which is calculated based on the residuals observed and simulated (from Eq. (2)) satellite data. For further details on the application of the PF for assimilating remotely sensed data, see DeChant and Moradkhani (2011a).

2.4. Drought initial conditions

The focus of this study is on drought throughout the UCRB on forecast starts dates of April 1st and July 1st of years 2003 through 2008. Drought will be characterized by deficits in the Land Water Storage (LWS), which is defined here as the sum of the soil moisture, to a depth of 1 meter, and the snow water equivalent. LWS is a useful quantity for examining drought because it represents all of the water stored above and immediately below the land surface, which is an important indicator of agricultural and hydrological drought. With respect to the drought status of the forecast initial conditions, Table 1 compares the LWS at each starting date. In this table, the spatially averaged LWS initial condition expected value from data assimilation is compared with the historical average from a historical VIC simulation (see Section 3.1). This table clearly shows that LWS at each forecast initialization date is below the average historical value, indicating drought conditions. Of these years, 2007 was found to be the worst drought for April over the entire basin, and 2006 was found to be the worst drought for July over the entire basin. Alternatively, the least intense drought year was 2003 for April and 2005 for July. This provides varying intensities of drought conditions for forecast initialization, allowing for comparison of drought recovery from different drought events.

3. Experimental setup

3.1. Climatology and forecast

The first simulation in this study is performed by running VIC for over the entire historical 30-year dataset, from April 1st 1981 through June 30th 2011. In order to generate climatology of land surface states, LWS values are sampled from each year of the historical simulation, providing an ensemble of 30 LWS values at each time step, over the forecast lead time, as shown in Eq. (4), where LWS_t^c represents the climatological distribution of LWS values at time t.

$$LWS_t^c = [LWS_{t,1}^c \quad LWS_{t,2}^c \quad \cdots \quad LWS_{t,30}^c] \tag{4}$$

This represents the forecast of greatest possible uncertainty, as it does not utilize information about the initial conditions or meteorological forcing beyond the historical record.

The second simulation is a forecasting experiment based on ESP, initialized with land surface states sampled from the data assimilation experiment described in Section 2.3, referred to as the forecast (DeChant and Moradkhani, 2011b). The forecast initial conditions were sampled from the posterior distribution estimated with data assimilation at the forecast start date, and then performs simulations from those states with meteorological forcing sampled from the 30 year dataset used to simulate climatology. 500 combinations of the initial conditions and meteorological forcing time series' were sampled randomly, and a forecast was generated from each of these combinations, thus creating an ensemble forecast of 500 members, as shown in Fig. 5.

$$LWS_t^f = [LWS_{t,1}^f \quad LWS_{t,2}^f \quad \cdots \quad LWS_{t,500}^f] \tag{5}$$

The forecast has increased information beyond climatology resulting from the land surface state initialization. As the forecast progresses in time, the information added to the forecast from these initial states will reduce over time, leading to the forecast approaching the climatological distribution, and therefore moving away from the initial drought conditions.

The climatology and forecast estimate the LWS over a lead time of 360 days. This provides an extended period which is assumed to be of sufficient lead time for forecasts to approach climatology, thus becoming insensitive to the initial drought conditions. These forecasts are performed from April 1st, to correspond with the date of peak snow water storage, and from July 1st, to correspond roughly to the date of peak soil moisture and minimal snow influence, for each year from 2003 through 2008. By forecasting for a 360 day period, initialized with states on April 1st and July 1st, the time and rate of recovery from drought conditions throughout the UCRB will be quantified for both snow dominated and non-snow dominated seasons. For the analysis here, the LWS is averaged in 10 day increments, which is performed to smooth out the daily noise in the LWS variable, leading to more consistent results. The 10 day increment was chosen based on a comparison of increments ranging from 1 to 30 days, with 10 being a balance of daily noise reduction and retaining sufficient temporal resolution.

Table 1
Basin-wide average land water storage initial condition, in mm, from each forecast starting date and the historical average. Each year displays a water storage state less than the historical average, indicating drier than average (drought) conditions.

Year	April 1st	July 1st
Average	190.62	118.00
2003	172.50	85.71
2004	137.35	87.76
2005	155.10	104.32
2006	125.85	73.86
2007	117.32	82.66
2008	132.31	84.60

3.2. Quantifying drought recovery lead time

This study works under the assumption that the basin has fully recovered from a drought at the lead time when the forecast and climatology ensembles become statistically indistinguishable, and therefore may be assumed to be identical. Given that the forecasts and climatology are statistically indistinguishable after a specific time, then one can conclude that the uncertainty in the forecast is entirely a result of the forcing at future times. If the uncertainty is entirely a result of the forcing at any time in the forecast, then the initial drought conditions are completely alleviated, as they no longer affect the hydrologic conditions in the basin. Note that both the climatology and forecasts are based on the same models, and therefore the effects of model error will be negligible. Such an analysis requires a hypothesis testing framework to determine if the forecast ensemble is significantly different from climatology at each 10 day period over the forecast lead time. In this study, a two-sample Kolmogorov–Smirnov (KS) test is used to compare the two distributions (Wolfe and Hollander, 1973), with an attempt to reject the null hypothesis that the forecast distribution is equivalent to climatology. Given that the analysis is unable to reject the null hypothesis, it will be assumed that the two distributions are equivalent, and therefore the forecast has entirely recovered from the drought conditions experienced at the initial forecast date.

Hypothesis testing with the KS test relies on the construction of an empirical CDF of two distributions, which is described for the climatological ensemble in Eq. (6).

$$F_{t,B}^c = \sum_{b=1}^{B}\sum_{i=1}^{N}\begin{cases} 1 & LWS_{t,i}^c \leqslant LWS_{t,b} \\ 0 & otherwise \end{cases} \tag{6}$$

In Eq. (6), the $F^c_{t,B}$ is the empirical CDF of the climatology at time t, which is estimated over B histogram bins distributed uniformly between the maximum and minimum value from the concatenated LWS^c_t and LWS^f_t arrays, N is the number of ensemble members (30 for climatology), and $LWS_{t,b}$ is the maximum LWS value for bin b at time t. Note that this is performed similarly for the forecast ensemble, which will be use the notation $F^f_{t,B}$. For the construction of both CDFs, B is set equal to 530 as it is the total number of data points in the concatenated LWS^c_t and LWS^f_t arrays.

After construction of the CDFs, the KS test examines the maximum absolute difference of the forecast and climatology CDFs across all bins, which then must be multiplied by the square root of the ratio of the product and sum of the forecast ($M = 500$) and climatology ($N = 30$) sample sizes, as shown in Eq. (7).

$$D_t = \max\left(\left|F^f_{t,1:B} - F^c_{t,1:B}\right|\right) \tag{7}$$

From this equation, the two-sample KS statistic (D_t) is estimated, which may be used for testing the null hypothesis. In this application, if D_t is greater than 0.2556, then the null hypothesis is rejected (with 95% confidence), and the forecast and climatological ensembles are considered different. At any time step in which the null hypothesis is not rejected, we can assume that the land surface conditions are not significantly different than climatology, thus showing that the basin is no longer experiencing drought conditions and completely insensitive to the initial drought conditions.

3.3. Quantifying drought recovery rate

This study also seeks to estimate the rate of drought recovery. Such an analysis is motivated by the complexity of drought recovery time, where the intensity of the initial drought and the speed at which the region rebounds from drought are important. Since drought recovery time is a function of both the initial LWS deficit and the rate at which that deficit is reduced, isolating the recovery rate may provide further insight into the factors determining drought recovery lead time. In order to estimate this rate, information theory provides a useful framework for examining the information provided by the initial drought states. Within information theory, entropy is a basic idea for examining the amount of information a probability distribution contains in respect to some random variable, which is typically estimated with Shannon Entropy (Shannon, 1948) (Eq. (8)).

$$H(LWS^c_t) = -\sum_{j=1}^{J} p(LWS^c_{t,j}) \log(p(LWS^c_{t,j})) \tag{8}$$

In Eq. (8), J is the number of LWS values at which the probabilities are estimated, $p(LWS^c_{t,j})$ is the probability of the LWS, according to the climatological ensemble, evaluated at time t and value j, $\log(p(LWS^c_{t,j}))$ is the natural logarithm of that probability, and $H(LWS^c_t)$ is the entropy at time t. From this definition, entropy is inversely proportional to information content of a given probability density, where a value approaching 0 indicates an increasingly informative forecast (low uncertainty) and a value approaching infinity indicates a decreasingly informative forecast (high uncertainty). Although the probabilities in Eq. (8) could be estimated from empirical distributions shown in Eq. (6), the small ensemble sizes will likely lead to biased entropy estimates (Miller, 1955), necessitating interpolation to regions of the LWS space unrepresented by the ensemble members. To ensure minimal bias, both the climatology and forecast ensembles are fit with a Kernel Smoothing Density to estimate the probability between ensemble members, as shown in Eqs. (9) and (10).

$$KS\left(LWS^c_{t,j}\right) = \frac{1}{Nh}\sum_{i=1}^{N} K\left(\frac{LWS^c_{t,i} - LWS_j}{h}\right) \tag{9}$$

$$p(LWS^c_{t,j}) = \frac{KS(LWS^c_{t,j})}{\sum_{j=1}^{J} KS(LWS^c_{t,j})} \tag{10}$$

In Eq. (9), N is the ensemble size, LWS_j is the value at which the probability is being estimated, h is the smoothing parameter, K is the kernel, which is chosen here as Gaussian, and $KS(LWS^c_{t,j})$ is the corresponding Kernel Smoothing Density estimate at time t and value j. This density is then normalized according to Eq. (10) to estimate the probability at that location and time. The probability is estimated at 1000 values (J), uniformly distributed between the minimum and maximum values of the concatenated LWS^c_t and LWS^f_t arrays. The smoothing parameter is estimated from Eq. (11), which is the optimal value for a Gaussian kernel, where σ is the standard deviation of LWS^c_t. This operation may be performed similarly for the forecast ensemble to estimate the information contained in the forecast.

$$h = \left(\frac{4\sigma^5}{3N}\right)^{1/5} \tag{11}$$

Beyond simply quantifying the amount of information in the climatology and forecast ensembles, the goal here is to estimate the amount of information that the forecast contains in relation to climatology. An important note is that these two ensembles quantify the same variable (LWS). Therefore, this study seeks to quantify the relative information loss of the forecast in comparison to climatology, which will therefore estimate the rate at which the forecast loses information extracted from the initial drought states, referred to here as the drought recovery rate. Within this scenario, the climatology has no information from initial drought status, but contains nearly identical information to the forecast with respect to meteorological forcing and model structure. Since the forecast will become insensitive to the initial drought status at some lead time, leading to the forecast and climatology having equivalent LWS distributions, the climatological distribution represents the minimum information content that the forecast will achieve. More specifically, the forecast has greater information content in the initial LWS than climatology (resulting from information extracted from the spin-up with data assimilation), and equivalent forcing information to climatology, allowing for the condition in Eq. (12). As noted in Eq. (12), the entropy of the forecast distribution will be less than climatology at all times, except at the time when the forecast and climatology become identical, due to the knowledge that entropy is inversely proportional to information content.

$$H(LWS^c_t) \geqslant H\left(LWS^f_t\right) \tag{12}$$

Since the entropy of the climatology will always be greater than or equal to the forecast, and the initial drought state is the only additional information source the forecast contains beyond the climatology, the fraction of the information extracted from the initial drought state by the forecast is equivalent to the ratio of the forecast and climatology entropies. This ratio is referred to as the relative entropy (RE), and is shown in Eq. (13).

$$RE_t = \frac{H\left(LWS^f_t\right)}{H\left(LWS^c_t\right)} \tag{13}$$

The RE (RE_t) ranges between 0 and 1, with 0 indicating all information in the forecast is derived from the initial drought conditions, and 1 indicating no information in the forecast is derived from the initial drought conditions. Therefore this study will estimate

rate of change of the relative entropy, which requires a function to be fit to the estimated RE data points.

Estimation of drought recovery rate is made difficult by the non-linear nature of the RE metric. Due to this non-linearity, and the upper limit of 1 for the RE value, this study will quantify the drought recovery rate by fitting an exponential function to the time series' of RE. A simple yet effective function is Eq. (14), where the least squares fit is deemed sufficient ($\min(\sum(RE_t - f_{RE}(t))^2)$).

$$f_{RE}(t) = 1 - \frac{1}{t^n} \tag{14}$$

In Eq. (14), t is the lead time in days. This function asymptotically approaches 1 for all positive n values, with increasing values indicating a faster rate of drought recovery. Throughout the analysis of the results, the exponent in Eq. (14) will be used to quantify drought recovery rate. Eq. (14) was chosen over other functions, specifically logarithmic or polynomial functions, because it produced the lowest squared error of the alternatives examined.

4. Results

4.1. Forecast initial conditions

An initial comparison of the forecast and climatology from each start date is provided in Figs. 2 and 3. In these figures, the spatially averaged median (dotted line) and 95% confidence bounds (solid lines) are shown for the forecast (red line) and climatology (blue line). This representation shows the progression of reducing forecast bias, and increasing width of the 95% predictive bounds, as climatology is approached. This indicates a slow loss of sensitivity to the forecast initial conditions, which is highly dependent on the drought intensity at the initial forecast date. For example, the forecast starting on July 1st 2005 clearly approaches climatology, and is indistinguishable from climatology by the end of the 360 day forecast. In addition, the July 2005 forecast approaches climatology in a much shorter lead time than all other forecasts, due to the proximity of the initial states to the climatological average. Alternatively, the forecast mean and 95% predictive bounds from April of 2007 do not appear to completely match climatology even at 360 days, which indicates an extended length recovery time from intense drought in the UCRB. Similar observation may be made from the July 2006 forecast, where the forecast required greater lead time to approach climatology than all other years. From a qualitative standpoint, Figs. 2 and 3 are very informative of the behavior of forecasts initialized at different drought intensities, but more detailed analysis requires the use of quantitative measures. As described earlier, the measures used here are the KS test and the RE.

4.2. Drought recovery lead time

The lead time at which the basin-wide LWS forecast ensemble becomes equivalent to climatological ensemble is quantified with the spatially averaged LWS forecasts, based on the results presented in Figs. 2 and 3. Through the KS test, the time at which the spatially averaged forecast and climatology become statistically inseparable is estimated, and is presented in Fig. 4. In this figure, the region shaded in black indicates that the distributions are significantly different, and the white region indicates that the forecast and climatology are statistically indistinguishable. Therefore, the time at which the figure transitions from black to white is the drought recovery lead time.

From Fig. 4, it is clear that the magnitude of LWS deficits at the initial forecast date affect the lead time required for recovery. For example, in 2005, forecasts starting in both April and July have their shortest time to recovery, about 6 and 3 months respectively, but display their longest recovery time in 2006, at around 9 months for both. Such a finding is intuitive, as increasingly severe droughts are expected to have increasingly long recovery times. One important note is that April 2003 has a spatially averaged LWS initial condition that is closer to climatology than April 2005, but has a slightly longer recovery time. This discrepancy is a result of a much greater concentration of water in snowpack in the high elevations regions in 2003 than 2005, indicating that spatial averages are useful in a general sense, but do not perfectly show the relationship between drought intensity and recovery time. Overall Fig. 4 suggests that spatially averaged LWS may take between 6 and 9 (3 and 9) months to recover from the drought conditions observed in April (July). These results suggest different sensitivities to initial conditions than previous studies. From conclusions in previous studies, one would likely assume that drought conditions in April would persist for a maximum lead time of 6 months (Shukla et al., 2013), while drought conditions in July would persist for a maximum lead time of around 3 months (Paiva et al., 2012). Interestingly, the maximum lead time of initial condition influence estimated from previous studies is similar to

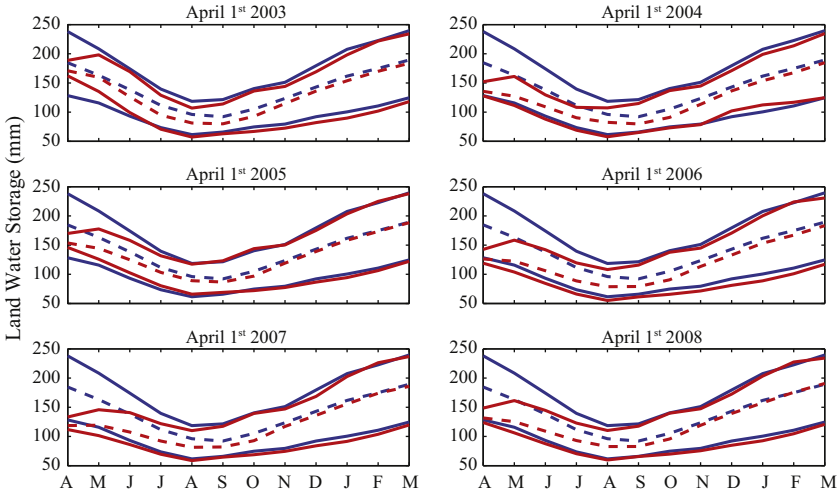

Fig. 2. Spatially averaged land water storage (soil moisture + snow water equivalent) for the upper Colorado River Basin, starting on April 1st. The median value is represented with the dotted lines and the 95% predictive intervals are represented with solid lines, with red representing the forecast and blue representing climatology. (For interpretation of the references to colour in this figure legend, the reader is referred to the web version of this article.)

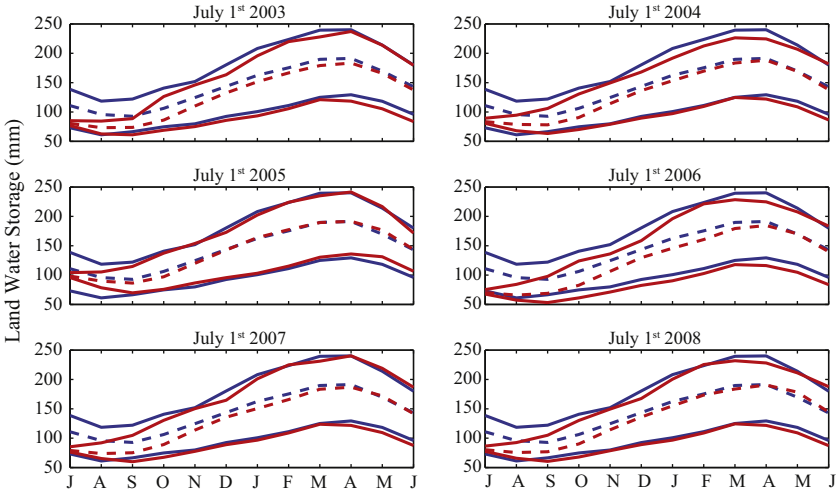

Fig. 3. Same as Fig. 2, but for all starting dates in July.

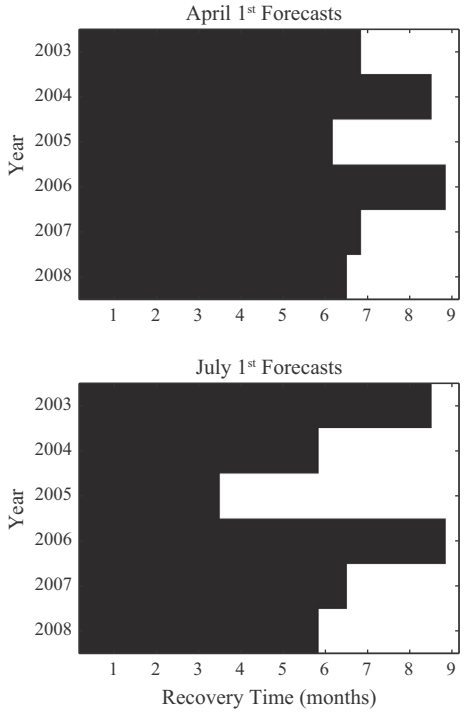

Fig. 4. Kolmogorov–Smirnov test for the spatially averaged land water storage, where black regions indicate that the forecast and climatology are significantly different, and white regions indicate the forecast and climatology are indistinguishable.

the minimum drought recovery time determined here. These differing results are explained by the varying perspectives between this study and previous studies. While previous studies examined the relative influence of initial conditions and forcing, this study quantified the lead time at which the initial conditions have no influence. This distinction is important for examining both drought recovery time, and the benefit of improving initial conditions in hydro-meteorological forecasts.

More detailed analysis of drought recovery lead time is performed by viewing spatial patterns of recovery time. Figs. 5 and 6 show the spatially distributed drought recovery lead times for the forecasts originating from April and July, respectively. A first observation from these maps is the extent of the basin which requires nearly the entire 360 day forecast period to recover (shown in red)[1]. For forecasts originating in both April and July, large regions in the interior of the UCRB are in deficit conditions throughout the 360 day lead time, with more intense drought years displaying greater recovery time. These interior regions are among the driest portions in the basin, and therefore this scenario may be explained by the difficulty of recovering from a drought when precipitation is sparse even during average climatic conditions. Alternatively, the northern and western portions of the UCRB have among the shortest drought recovery lead times, with some regions reaching climatology within a few months. Due to the increased precipitation in these regions, and the magnitude of typical snow water storage in relation to soil moisture, drought recovery can be quite rapid. Since the LWS in these regions is dominated by snow, it is unlikely that a drought could take more than one year for recovery under normal climatic conditions, due to near complete melt every year, resulting in a clean start after every summer. Alternatively, the LWS in the central portions is dominated by soil moisture, and therefore the memory in this region has the potential to be much longer, as the soil moisture will never reach zero.

Further patterns may be observed when comparing April and July forecasts. From Figs. 5 and 6, it is clear the July forecasts tend to have shorter drought recovery times in the southern portion of the UCRB, but longer drought recovery times in the northern portion, as compared to the April forecasts. This issue likely has less to do with initial drought status as it does with normal precipitation timing in the central portions of the basin. Although the northern and higher elevation regions receive the vast majority of precipitation during the winter, the southern and interior portions receive a slightly larger portion of precipitation during the summer than in the winter, and therefore some regions have faster recovery times in July than April. An important note here is that this study assumes normal climate conditions over the forecast period, but in the central regions of this basin that assumption is potentially violated. Since much of the summer rains in this basin are due to thunderstorms resulting from moisture emanating from the North American Monsoon (Adams and Comrie, 1997), and moisture over southern portions of the basin and Arizona affecting atmospheric feedbacks (Feng et al., 2013), drought recovery time estimated for the south-central portion of the UCRB in this study may be very conservative. More robust analysis would require a coupled

[1] For interpretation of color in Figs. 5 and 6, the reader is referred to the web version of this article.

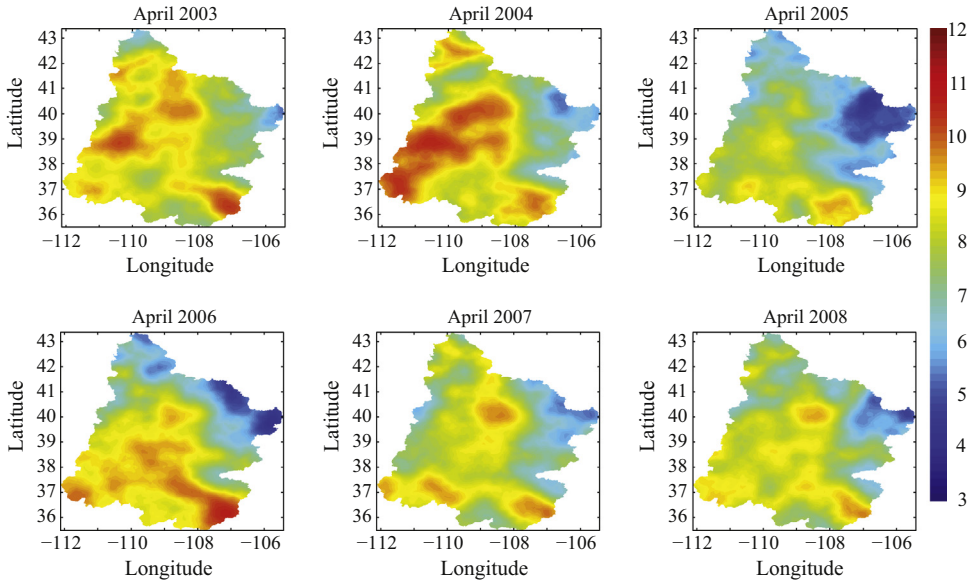

Fig. 5. Spatially distributed drought recovery time in the upper Colorado River Basin, starting on April 1st of each year, measured in months.

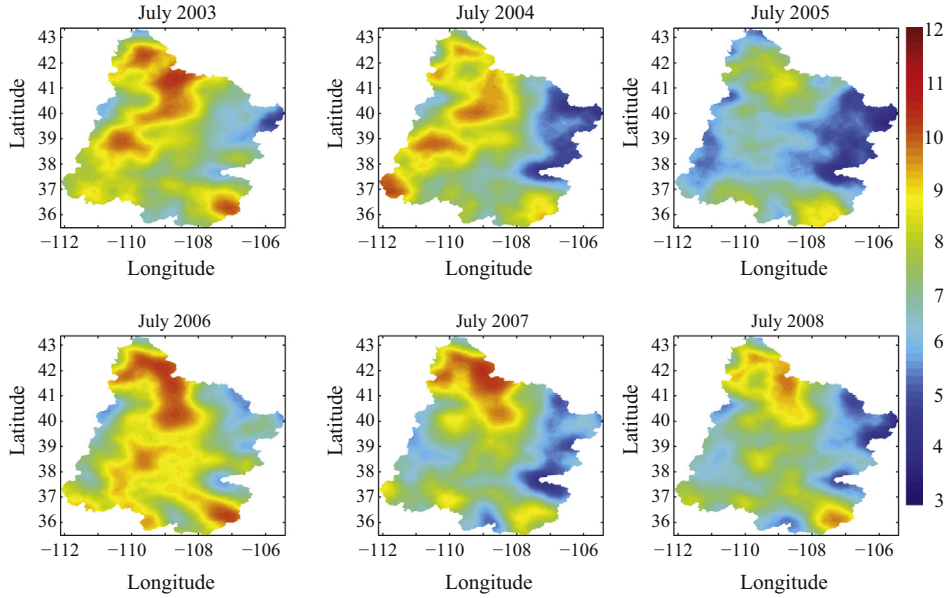

Fig. 6. Spatially distributed drought recovery time in the upper Colorado River Basin, starting on July 1st of each year, measured in months.

land–atmosphere model, which is outside the scope of this study, as the predominant source of water in the UCRB is the winter and spring westerly storm pattern.

4.3. Drought recovery rate

This manuscript has examined the recovery time from different drought conditions, but to further the analysis, it is important to understand the rate at which drought recovers. Such an analysis allows for separating the factors that determine recovery time (intensity and recovery rate). Whereas the time for drought recovery is highly dependent on drought intensity at the initial forecast date, the rate of drought recovery may be independent of the initial drought intensity. An example of this point is displayed in Fig. 7. In this figure, the RE of the spatially averaged LWS is plotted, with respect to time, and a line is fit to the data points from Eq. (11). From these results, it is clear that the variance in the rate of drought recovery is relatively constant, as the fitted lines differ only slightly from year to year. In addition, the rate of recovery shows very little variance between the two forecast start dates examined in this study, as shown in Table 2. All spatially averaged LWS RE functions had an exponent between 0.57 and 0.6, yet spatially distributed calculations ranges from 0.2 to 0.9 (Fig. 8). This contrasts with spatially averaged drought recovery time, which shows more temporal variability according to Fig. 4. From Fig. 8, April forecasts tend to have slightly larger variance in drought recovery rates, but overall the variability seems greater spatially than with respect to initial forecast date. In addition, the distributions of recovery rates from Fig. 8 have similar qualities, with an exponent value of around 0.45 having the greatest frequency in each month, and each distribution being positively skewed. This suggests that drought recovery rates from these months have

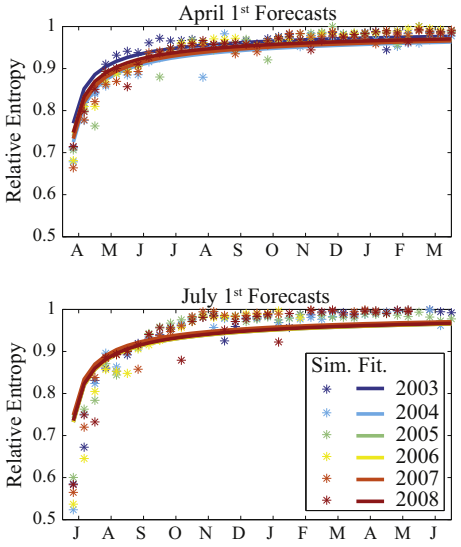

Fig. 7. Spatially averaged relative entropies (asterisks), with the fitted (lines) from Eq. (14), of the land water storage simulations with respect to climatology.

Table 2
Rate of drought recovery from each forecast initialization date, as estimated by the exponent (n) from Eq. (14).

Year	April 1st	July 1st
2003	0.64	0.57
2004	0.56	0.58
2005	0.58	0.59
2006	0.6	0.57
2007	0.57	0.6
2008	0.6	0.58

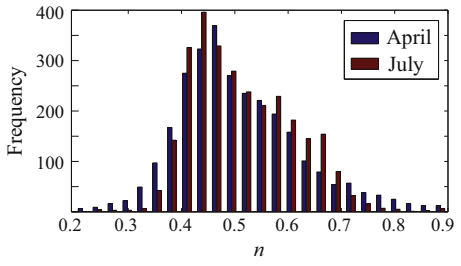

Fig. 8. Histogram of the spatially distributed exponent (n) values from Eq. (14). Increasing n indicates faster recovery rate.

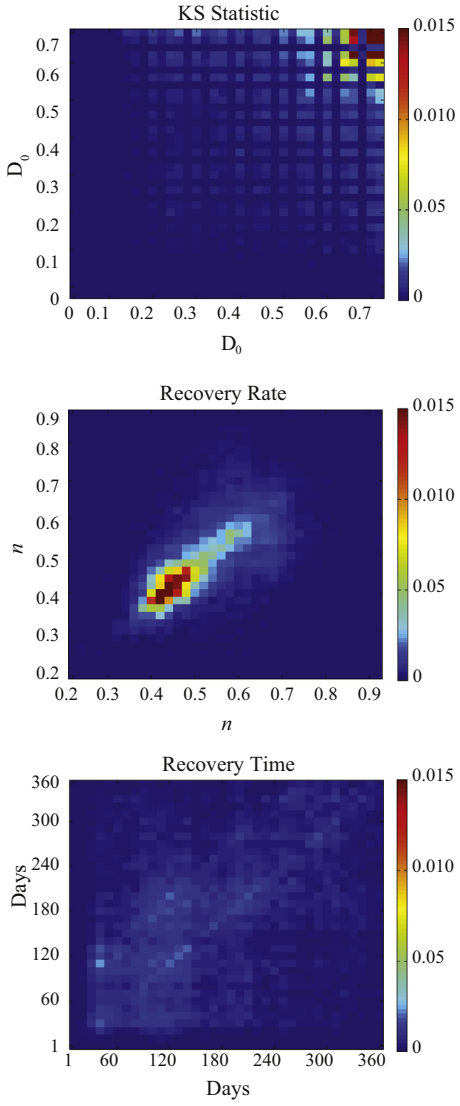

Fig. 9. Comparison of the consistency of the KS Statistic, the recovery rate and the recovery time estimates for each model cell. In these sub-plots, blue indicates rare combinations of values from different start dates, whereas red indicates frequent combinations of values from different start dates, as indicated by the colorbar on the right. (For interpretation of the references to colour in this figure legend, the reader is referred to the web version of this article.)

similar spatial patterns, and therefore the specific initial conditions may not have strong influence over the rate of recovery. Further analysis requires a direct comparison of the drought recovery time and rates.

Fig. 9 compares the KS test statistic for the initial conditions (D_0), which is a measurement of the distance between the initial forecast LWS and climatology, the drought recovery rate and the drought recovery time, for different forecast start dates. In this figure, each combination of D_0 (left subplot), recovery rate (middle subplot), and recovery time (right subplot) between two different start dates (66 unique combinations from the 12 starting dates), for each model grid cell, were plotted. For example, the D_0 value estimated for the each cell starting in April 1st 2003 is the y component, and the D_0 value estimated for the each cell starting in April 1st 2004 is the x component, for the first combination in the left subplot. Also, the D_0 values display vertical and horizontal lines, indicating values that are rarely estimated. These lines are a result of the climatology sample size (30) limiting the values that D_0 can take. Each subsequent combination of start dates is plotted as well, leading to 31,218 data points from the 66 combinations and 473 model grid cells. By comparing these three subplots, it is clear that the drought recovery rate shows a much more consistent pattern than D_0 values and drought recovery time. This consistent pattern for recovery rate shows a near linear correlation, which suggests nearly static values for a given location between different start dates. Alternatively, the D_0 value and drought recovery time is much more scattered, suggesting that the initial conditions and recovery time are more dynamic for a given location. Given the relationship between these two variables, it appears that initial condition variability is the primary driver in variability of the recovery time. In addition, the recovery rate is largely independent of the initial LWS, and therefore drought recovery rate is primarily controlled by the physical setting of the drought. Such results highlight the importance of the land surface characteristics of the

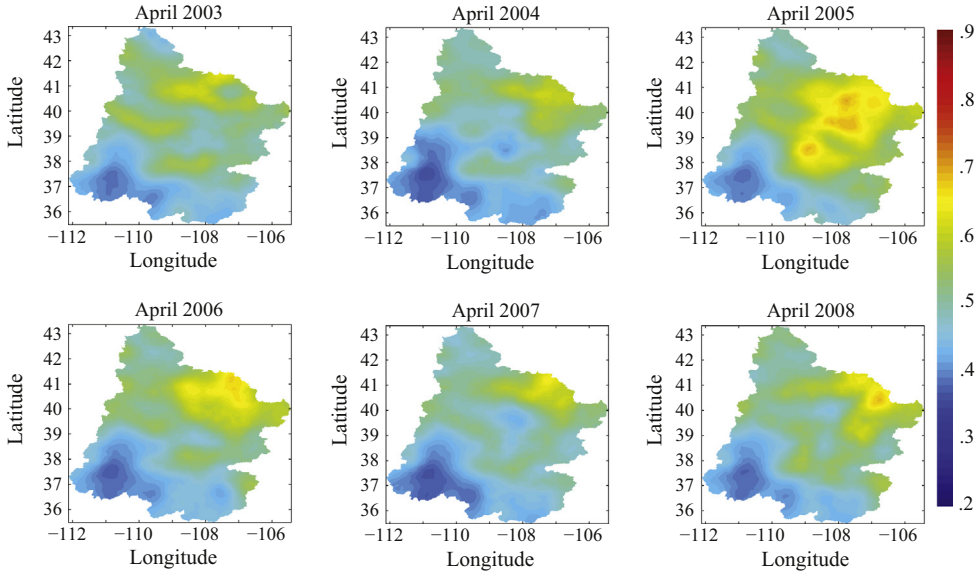

Fig. 10. Spatially distributed drought recovery rate in the upper Colorado River Basin, starting on April 1st of each year. Drought recovery rate is estimated as the exponent (n) of Eq. (14) after being fitted to the relative entropy time series of each grid cell. Larger n values indicate faster recovery rate.

region affected by drought, and not just the moisture deficit at a given time. Since the drought recovery rate is not significantly changing temporally, as evidenced by Fig. 9, yet there is a large range of drought recovery rates experienced in the basin, as shown in Fig. 8, it is important to examine the spatial distribution of drought recovery rates to determine drought prone regions.

The spatial distribution of drought recovery rates is displayed in Figs. 10 and 11. As was expected from Fig. 8, these rates are highly variable. In the April forecasts, drought recovery rates tend to be faster in the central to northeastern portions of the basin, and slower in the southern and western portions of the basin. As for July, the fastest drought recovery rates are primarily located in the far eastern portion of the basin, and other portions display a generally slow rate of drought recovery. Starting in both forecast months, the eastern portions of the basin recover from droughts the most rapidly, indicating that this region readily recovers from drought, making this the least drought prone region. Alternatively, the southern and western portions of the basin recover from drought very slowly, indicating that these regions are prone to extended drought conditions. This figure clearly shows that the rate of drought recovery is regional, and therefore is strongly affected by the geographical setting. In this study, the spatial variability in the simulations is caused by differing land surface parameters, indicating that land surface properties (soil types and vegetation cover) strongly affect the ability of a region to recover from drought.

4.4. Discussion and conclusions

This manuscript detailed a study of drought recovery forecasting, under the assumption of normal climate following a drought event. Rather than comparing the relative influence of initial conditions and forcing, the presented study examined the amount of time for the forecast to become insensitive to drought initial

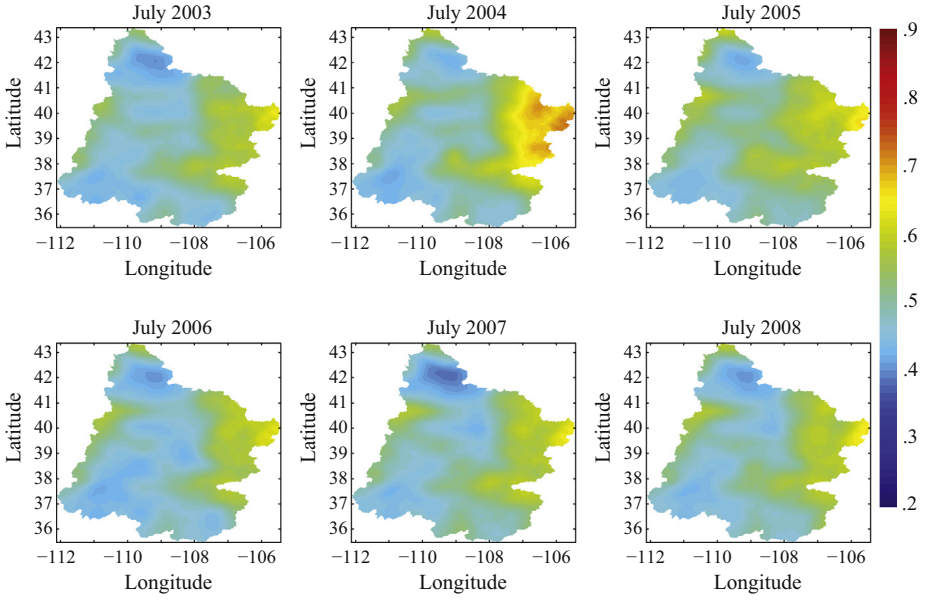

Fig. 11. Spatially distributed drought recovery rate in the upper Colorado River Basin, starting on July 1st of each year. Drought recovery rate is estimated as the exponent (n) of Eq. (14) after being fitted to the relative entropy time series of each grid cell. Larger n values indicate faster recovery rate.

conditions, and the rate at which a forecast loses sensitivity to the drought initial conditions. Such an examination is a proxy for estimating lead time, and rate, of drought recovery. Through the quantification of drought recovery time and rate, this study simultaneously provides insight into the expected behavior of the UCRB during the recession period of droughts, and the importance of precisely estimating initial conditions in forecasts of up to one year. Not surprisingly, this study found that drought recovery time was related to drought intensity, with increasing intensity requiring greater recovery time. Further, drought recovery time was found to be greater for forecasts originating in April than July, but the difference is smaller than anticipated. In some years, the overall basin recovery from forecasts originating in April and July were similar, whereas other years displayed a difference of up to three months. In general, one would assume that the April forecasts would have greater influence on drought recovery time, due to the presence of snow water storage, but this is not necessarily the case.

Results from this study clearly contrast with previous work, which is related to the differing perspectives on the importance of drought initial conditions. Due to previous studies focusing on lead time at which forcing becomes the dominant factor, in relation to initial conditions, and this study is seeking to quantify the lead time at which initial states significantly impact the forecast, sensitivity to initial conditions was found to be greater here than in other studies. A maximum of six months of sensitivity was generally found in previous studies, but results here suggest that a forecast may be sensitive to initial conditions beyond one year for select locations, but up to nine months at the basin scale. Further, this study shows that forecasts are sensitive to soil moisture at a minimum of three months, but previous studies generally suggested a maximum of three months. Overall these results suggest that initial conditions are potentially important in forecasts of greater lead time than previously thought. This finding suggests that data assimilation systems may have some benefit to forecasts at even a year lead time, although the importance of improved initial conditions will be less than forcing improvements beyond six months, as indicated by previous studies (Li et al., 2009; Mahanama et al., 2011; Paiva et al., 2012; Shukla and Lettenmaier, 2011; Shukla et al., 2013; Wood and Lettenmaier, 2008; Yossef et al., 2013). One drawback of this study is the limited number of forecast initialization dates (April 1st and July 1st for years 2003–2008) and small study area, and therefore more extensive studies are suggested, with the methods described in Section 3.2, to further examine the sensitivity of forecasts to initial conditions over more climatic regimes.

Drought recovery times estimated in this study should be treated as conservative. The results presented are based on initial conditions with large uncertainty. Through the data assimilation framework used here, initial conditions remain quite uncertain, resulting from the large uncertainty in the land surface model and remotely sensed observations. Since the initial conditions have large uncertainty, and hence less information about the initial conditions than precise estimates, the forecasts examined here lose sensitivity to the initial conditions more rapidly than precise estimate would. Assuming that land surface modeling and remote sensing science progresses to allow data assimilation to decrease initial condition uncertainty, the lead time at which a forecast becomes insensitive to initial conditions will increase. This knowledge further motivates the use of data assimilation for initializing forecasts of extended length as it will reduce the uncertainty in the initial condition, thus increasing the information added to the forecast from the initial conditions.

A final conclusion from this study is the difference between drought recovery time and rate of recovery. Since the drought recovery time is highly dependent on initial conditions, this value varies strongly temporally. Alternatively, the drought recovery rate appears to be more related to the specific location than drought intensity. This is evidenced by the temporal similarity of drought recovery rates, as shown in Fig. 9, and the spatial similarity of drought recovery rates, as shown in Figs. 10 and 11. This conclusion gives some insight into the geographic settings in which drought is most persistent. In the mountainous northeastern region of the UCRB, droughts recover quickly, yet the low lying southern and western regions recover slowly from drought. Drought mitigation within the drier regions of the UCRB is therefore a much greater challenge than in the mountainous regions. Fortunately, the total runoff from this basin is dominated by flow from mountainous regions, and therefore total basin water storage is expected to recover at a rate faster than that of the dry interior portions.

Acknowledgement

This study was supported by NOAA-MAPP (NA11OAR4310140).

References

Adams, D.K., Comrie, A.C., 1997. The North American Monsoon. Bull. Am. Meteorol. Soc. 78 (10), 2197–2213.
Andreadis, K.M., Lettenmaier, D.P., 2006a. Trends in 20th century drought over the continental United States. Geophys. Res. Lett. 33 (10), L10403.
Andreadis, K.M., Lettenmaier, D.P., 2006b. Assimilating remotely sensed snow observations into a macroscale hydrology model. Adv. Water Resources, 29, 872–873–886.
Bras, R.L., 1990. Hydrology: an Introduction to Hydrologic Science, edited, Addison-Wesley, Workingham, pp. 188–241.
Brown, J.D., Demargne, J., Seo, D.-J., Liu, Y., 2010. The Ensemble Verification System (EVS): a software tool for verifying ensemble forecasts of hydrometeorological and hydrologic variables at discrete locations. Environ. Modell. Softw. 25 (7), 854–872.
Clark, M.P., Rupp, D.E., Woods, R.A., Zheng, X., Ibbitt, R.P., Slater, A.G., Schmidt, J., Uddstrom, M.J., 2008. Hydrological data assimilation with the ensemble Kalman filter: use of streamflow observations to update states in a distributed hydrological model. Adv. Water Resour. 31, 1309.
Daly, C., Neilson, R.P., Phillips, D.L., 1994. A statistical-topographic model for mapping climatological precipitation over mountainous terrain. J. Appl. Meteorol. 33 (2), 140–158.
De Lannoy, G.J.M., Reichle, R.H., Arsenault, K.R., Houser, P.R., Kumar, S., Verhoest, N.E.C., Pauwels, V., 2012. Multiscale assimilation of Advanced Microwave Scanning Radiometer–EOS snow water equivalent and Moderate Resolution Imaging Spectroradiometer snow cover fraction observations in northern Colorado. Water Resour. Res. 48 (1).
Dechant, C., Moradkhani, H., 2011a. Radiance data assimilation for operational snow and streamflow forecasting. Adv. Water Resour. 34 (3), 351–364.
DeChant, C.M., Moradkhani, H., 2011b. Improving the characterization of initial condition for ensemble streamflow prediction using data assimilation. Hydrol. Earth Syst. Sci. 15 (11), 3399–3410.
DeChant, C.M., Moradkhani, H., 2014, Toward a reliable prediction of seasonal forecast uncertainty: addressing model and initial condition uncertainty with ensemble data assimilation and sequential bayesian combination, J. Hydrol., Special Issues on Ensemble Forecasting and Data Assimilation, 519 (PD), 2967–2977.
Demargne, J., Wu, L., Regonda, S., Brown, J., Lee, H., He, M., Seo, D.-J., Hartman, R., Herr, H.D., Fresch, M., 2013. The science of NOAA's operational hydrologic ensemble forecast service. Bulletin Am. Meteorol. Soc.
Durand, M., Molotch, N.P., Margulis, S.A., 2008. A Bayesian approach to snow water equivalent reconstruction. J. Geophys. Res. 113 (D), 20117.
Feng, X., Bosilovich, M., Houser, P., Chern, J.D., 2013. Impact of land surface conditions on 2004 North American monsoon in GCM experiments. J. Geophys. Res.: Atmospheres.
Franz, K.J., Hogue, T.S., Sorooshian, S., 2008. Snow model verification using ensemble prediction and operational benchmarks. J. Hydrometeorol. 9 (6), 1402–1415.
Gao, H., Tang, Q., Shi, X., Zhu, C., Bohn, T.J., Su, F., Sheffield, J., Pan, M., Lettenmaier, D.P., Wood, E.F., 2010. Water budget record from Variable Infiltration Capacity (VIC) model. Algorithm Theor. Basis Document Terrestrial Water Cycle Data Rec.
Hao, Z., AghaKouchak, A., 2013. A nonparametric multivariate multi-index drought monitoring framework. J. Hydrometeorol. 15 (1), 89–101.
Huang, W.C., Chou, C.C., 2008. Risk-based drought early warning system in reservoir operation. Adv. Water Resour. 31 (4), 649–660.
Kalnay, E., Kanamitsu, M., Kistler, R., Collins, W., Deaven, D., Gandin, L., Iredell, M., Saha, S., White, G., Woollen, J., 1996. The NCEP/NCAR 40-year reanalysis project. Bull. Am. Meteorol. Soc. 77 (3), 437–471.

Kimball, J.S., Running, S.W., Nemani, R., 1997. An improved method for estimating surface humidity from daily minimum temperature. Agric. For. Meteorol. 85 (1), 87–98.
Leisenring, M., Moradkhani, H., 2011. Snow water equivalent prediction using Bayesian data assimilation methods. Stoch. Env. Res. Risk Assess. 25 (2), 253–270.
Li, H., Luo, L., Wood, E.F., Schaake, J., 2009. The role of initial conditions and forcing uncertainties in seasonal hydrologic forecasting. J. Geophys. Res.: Atmospheres 114 (D4), D04114.
Liang, X., Lettenmaier, D.P., Wood, E.F., Burges, S.J., 1994. A simple hydrologically based model of land surface water and energy fluxes for general circulation models. J. Geophys. Res. 99 (D7), 14415.
Madadgar, S., Moradkhani, H., 2013a. Drought analysis under climate change using 636 copula. J. Hydrol. Eng. 18 (7), 637. http://dx.doi.org/10.1061/(ASCE)HE.1943-5584.0000532.
Madadgar, S., Moradkhani, H., 2013b. A Bayesian framework for probabilistic seasonal drought forecasting. J. Hydrometeorol. 14 (6), 1685–1705.
Madadgar, S., Moradkhani, H., 2014. Spatio-temporal drought forecasting within Bayesian networks. J. Hydrol. 512, 134–146.
Mahanama, S., Livneh, B., Koster, R., Lettenmaier, D., Reichle, R., 2011. Soil moisture, snow, and seasonal streamflow forecasts in the United States. J. Hydrometeorol. 13 (1), 189–203.
Maity, R., Ramadas, M., Govindaraju, R.S., 2013. Identification of hydrologic drought triggers from hydroclimatic predictor variables. Water Resour. Res. 49 (7), 4476–4492.
Margulis, S.A., McLaughlin, D., Entekhabi, D., Dunne, S., 2002. Land data assimilation and estimation of soil moisture using measurements from the Southern Great Plains 1997 Field Experiment. Water Resour. Res. 38 (12), 35-31.
Maurer, E.P., Wood, A.W., Adams, J.C., Lettenmaier, D.P., Nijssen, B., 2002. A long-term hydrologically-based data set of land surface fluxes and states for the conterminous United States. J. Clim. 15, 3237.
Miller, G.A., 1955. Note on the bias of information estimates. Inform. theory psychol.: Probl. meth. 2, 95–100.
Mishra, A.K., Singh, V.P., 2010. A review of drought concepts. J. Hydrol. 391, 202–216.
Mo, K.C., Chen, L.-C., Shukla, S., Bohn, T.J., Lettenmaier, D.P., 2012. Uncertainties in North American land data assimilation systems over the contiguous United States. J. Hydrometeorol. 13 (3), 996–1009.
Paiva, R.C.D., Collischonn, W., Bonnet, M.-P., Gonçalves, L. G. G. d., 2012. On the sources of hydrological prediction uncertainty in the Amazon. Hydrol. Earth Syst. Sci. 16 (9), 3127–3137.
Pan, M., Yuan, X., Wood, E.F., 2013. A probabilistic framework for assessing drought recovery. Geophys. Res. Lett. 40 (14), 3637–3642.
Pozzi, W. et al., 2013. Toward global drought early warning capability: expanding international cooperation for the development of a framework for monitoring and forecasting. Bull. Am. Meteorol. Soc. 94 (6), 776–785.
Pulliainen, J. et al., 1998. Retrieval of geophysical parameters with integrated modeling of land surfaces and atmosphere (models/inversion algorithms): Final report. Helsinki University of Technology, Laboratory of Space Technology.
Reichle, R.H., McLaughlin, D.B., Entekhabi, D., 2002. Hydrologic data assimilation with the ensemble Kalman filter. Mon. Weather Rev. 130 (1), 103–114.
Shannon, C.E., 1948. A mathematical theory of communication. AT&T Tech. J. 27 (3), 379–423. http://dx.doi.org/10.1002/j.1538-7305.1948.tb01338.x.
Shukla, S., Lettenmaier, D.P., 2011. Seasonal hydrologic prediction in the United States: understanding the role of initial hydrologic conditions and seasonal climate forecast skill. Hydrol. Earth Syst. Sci. 15 (11), 3529–3538.
Shukla, S., Sheffield, J., Wood, E.F., Lettenmaier, D.P., 2013. On the sources of global land surface hydrologic predictability. Hydrol. Earth Syst. Sci. 17 (7), 2781–2796.
Thornton, P.E., Running, S.W., 1999. An improved algorithm for estimating incident daily solar radiation from measurements of temperature, humidity, and precipitation. Agric. For. Meteorol. 93 (4), 211–228.
Wiesmann, A., Mätzler, C., 1999. Microwave emission model of layered snowpacks. Remote Sens. Environ. 70 (3), 307–316.
Wigneron, J.P. et al., 2007. L-band microwave emission of the biosphere (L-MEB) model: description and calibration against experimental data sets over crop fields. Remote Sens. Environ. 107 (4), 639–655.
Wolfe, D.A., Hollander, M., 1973. Nonparametric statistical methods. Nonparametric statistical methods, John Wiley New York.
Wood, A.W., Lettenmaier, D.P., 2008. An ensemble approach for attribution of hydrologic prediction uncertainty. Geophys. Res. Lett. 35 (14), L14401.
Yossef, N.C., Winsemius, H., Weerts, A., van Beek, R., Bierkens, M.F.P., 2013. Skill of a global seasonal streamflow forecasting system, relative roles of initial conditions and meteorological forcing. Water Resour. Res. 49 (8), 4687–4699.
Yuan, X., Wood, E.F., Chaney, N.W., Sheffield, J., Kam, J., Liang, M., Guan, K., 2013. Probabilistic seasonal forecasting of african drought by dynamical models. J. Hydrometeorol.